PCCP

ROYAL SOCIETY OF CHEMISTRY

PAPER

View Article Online
View Journal | View Issue

Cite this: *Phys. Chem. Chem. Phys.*, 2024, **26**, 5207

The role of pressure on lattice thermal conductivity and its related thermodynamical parameters in $In_{0.53}Ga_{0.47}As$ nanofilms

N. A. Rauf * and M. S. Omar

Received 24th November 2023,
Accepted 22nd December 2023

DOI: 10.1039/d3cp05729a

rsc.li/pccp

Lattice thermal conductivity (LTC) for $In_{0.53}Ga_{0.47}As$ alloy films, with thicknesses ranging from 10 nm to 1.4 μm, was investigated under pressures of up to 11 GPa and temperatures between 1 and 450 K, utilizing the modified Debye–Callaway model. The effects of structural and thermodynamical parameters, as well as phonon interactions, on LTC were examined. The Clapeyron, Murnaghan, and Post equations were applied to determine the pressure dependence of the melting temperature, lattice volume, and Debye temperature, respectively. A novel derivative form of the bulk modulus, suitable for nanomaterials, has been introduced. It was found that decreasing the film thickness increases the Gruneisen parameter, while increasing pressure decreases it. The LTC of nanofilms is significantly affected by their thickness and pressure strength; notably, under 11 GPa, films with a thickness of 10 nm exhibit a substantial decrease in LTC. LTC_{max} declines due to the greater influence of boundary scattering compared to dislocations. These findings suggest potential applications in managing nanofilm temperature and size, which are key to advancing nanomaterials and enhancing the efficiency of electronic devices.

1. Introduction

In recent decades, researchers have focused on the thermal conductivity of nanostructured materials[1,2] due to its direct relation to the efficiency of thermal dissipation. Accurate calculation of lattice thermal conductivity is crucial for designing high-quality nano-electronic[3] power devices,[4,5] generating transistors,[6] and thermoelectric generators. Hydrostatic pressure serves as a principal thermodynamic variable used to accelerate reactions, design novel structures, and define the properties of nanostructures.[7,8] Pressure is a significant factor in semiconductor behavior, meriting further study.[9] The alloy $In_{0.53}Ga_{0.47}As$, formed from InAs and GaAs, has a zinc blende structure with a lattice parameter $a(\infty)$ of 5.868 Å[10] and a direct band gap, making it suitable for high-performance photodiodes.[11] Its nanofilms are versatile, and used in devices for their radiation resistance and durability.[12] The alloy's applications now include lasers,[13] photodetectors,[14] transistors,[5,15] and photovoltaics,[5,15] with transistors being prevalent in modern electronics like smartphones and computers.

Pressure's impact on thermal conductivity[16] is key for understanding phase transitions and material properties, and is studied both theoretically and experimentally. The process is vital in fields such as astrophysics and geosciences. Many authors have predicted theoretical calculations of the pressure effect on size-dependent LTC in InAs nanowires, Si nanofilms, and multilayer hexagonal boron nitride.[17–19] Theoretical models predict how pressure affects the lattice thermal conductivity (LTC) in various nanostructures, aiding in the design and analysis of their physical and thermal properties.[7] For $In_{0.53}Ga_{0.47}As$ nanofilms, such analysis is crucial as it allows for precise LTC calculations under pressure. However, for validating these results, experimental data exist only for the zero pressure LTC of $In_{0.53}Ga_{0.47}As$ films (10 nm–1.4 μm),[5,20] making these findings useful for overcoming experimental challenges in other pressure ranges of up to 11 GPa, where the challenges could range from technical and financial constraints. The Clapeyron model, utilized in this work, is preferred due to its broad application in analyzing phase transitions, such as melting, because it describes how pressure affects the melting temperature. It is now also applicable at the nanoscale.[17–19] In contrast, other used models, *e.g.* the DNA melting model, are specifically designed for DNA's thermal denaturation, considering nucleotide sequences and hydrogen bonds. The Clapeyron model predicts shifts in melting temperature with changes in pressure along phase boundaries, while the DNA model's temperature is determined by the genetic composition and stability of the DNA strands.[21–24]

Department of Physics, College of Science, Salahaddin University-Erbil, Erbil, 44001, Iraq. E-mail: nssar.rauf@su.edu.krd

In this work, the size-dependent LTC for $In_{0.53}Ga_{0.47}As$ nanofilms will be determined by using the modified Debye–Callaway model with the effects of hydrostatic pressure depending on the Murnaghan lattice parameter.[25] The Clapeyron equation for melting temperature T_m,[23,24] the Gruneisen parameter γ, which is derived from the Rice equation of measuring shock-waves,[26,27] the average phonon group velocity v^{ave},[28] Debye temperature θ_D,[29] surface energy σ_{sl}[24] and surface stress f_{sl},[30] and the bulk modulus B[31] with its first derivative B' representing new values appropriate for $In_{0.53}Ga_{0.47}As$ nanofilms, have been determined through a fresh derivation of the nanomaterial form. This approach was initially utilized by Hofmeister in 2002 for bulk materials.[32] On the assumption that the dimensions at the nanoscale do not have an impact on impurities and electronic behavior, a size-dependent density ρ[31] is calculated for all the film's thicknesses. This work examines how the lattice thermal conductivity (LTC) of nanofilms is influenced by their thickness and the amount of pressure they can withstand. In practical terms, these insights could lead to more efficient thermal management in electronic devices, as $In_{0.53}Ga_{0.47}As$ is known for its semiconductor properties. The potential implications include improved performance and reliability in high-tech applications, such as faster processors[33] and advanced sensors.[33]

2. Methods of calculation

The Debye–Callaway model that is modified by Asen-Palmer *et al.*[34] and Morelli *et al.*[35] is used to determine the LTC in $In_{0.53}Ga_{0.47}As$ bulk (thick) and nanofilms. The model includes both modes of one longitudinal K_L and two degenerate transverse (K_T) phonon branches, whilst acoustic phonon branches mostly contribute to heat conduction in semiconductors.[36,37] The temperature dependence of LTC in solids can be expressed as:[35]

$$K = K_L + 2K_T, \tag{1}$$

$$K_L = K_{L1} + K_{L2}, \tag{2}$$

$$K_T = K_{T1} + K_{T2}, \tag{3}$$

where transverse and longitudinal branches are denoted by T and L, respectively. The partial conductivity term of the modified Debye–Callaway model can be given by K_{L1} and K_{L2}, as in the following form:[35]

$$K_{L1} = \frac{1}{3}A_L T^3 \int_0^{\frac{\theta_D^L}{T}} \tau_C^L(x) z(x) \mathrm{d}x, \tag{4}$$

$$K_{L2} = \frac{1}{3}A_L T^3 \left[\int_0^{\frac{\theta_D^L}{T}} \frac{\tau_C^L(x)}{\tau_N^L(x)} z(x)\mathrm{d}x\right]^2 \times \left[\int_0^{\frac{\theta_D^L}{T}} \frac{\tau_C^L(x)}{\tau_N^L(x)\tau_R^L(x)} z(x)\mathrm{d}x\right]^{-1} \tag{5}$$

The transverse contribution has two forms, which are as follows:

$$K_{T1} = \frac{1}{3}A_T T^3 \int_0^{\frac{\theta_D^T}{T}} \tau_C^T(x) z(x) \mathrm{d}x, \tag{6}$$

$$K_{T2} = \frac{1}{3}A_T T^3 \left[\int_0^{\frac{\theta_D^T}{T}} \frac{\tau_C^T(x)}{\tau_N^T(x)} z(x)\mathrm{d}x\right]^2 \times \left[\int_0^{\frac{\theta_D^T}{T}} \frac{\tau_C^T(x)}{\tau_N^T(x)\tau_R^T(x)} z(x)\mathrm{d}x\right]^{-1}, \tag{7}$$

$$A_{L(T)} = \left(\frac{k_B}{\hbar}\right)^3 \left(\frac{k_B}{2\pi^2 v^{L(T)}}\right) \tag{8}$$

where $z(x) = x^4 e^x (e^x - 1)^{-2}$, $x = \dfrac{\hbar\omega}{k_B T}$, $\hbar$, k_B, T, v and ω are the Planck constant (1.05457×10^{-34} J s), Boltzmann's constant (1.38065×10^{-23} m^2 kg s^{-2} K^{-1}), absolute temperature, acoustic phonon group velocity and phonon frequency, respectively. The combined phonon-scattering is denoted by $\tau_C(x)$,[38] while $\tau_R(x)$ is the resistive total scattering. Furthermore, both branches of Debye temperature are determined by $\theta_D^{L(T)}$:[35]

$$\theta_D^{L(T)} = \left(\frac{\omega^{L(T)}\pi^2}{V}\right)^{\frac{1}{3}} \left(\frac{\hbar v^{L(T)}}{k_B}\right), \tag{9}$$

while the dispersion of phonon branches near the zone boundary is ignored. The resistive scattering processes $(\tau_R^{L(T)})^{-1}$ are estimated by:[20]

$$(\tau_R^{L(T)})^{-1} = (\tau_U^{L(T)})^{-1} + (\tau_M^{L(T)})^{-1} + (\tau_b^{L(T)})^{-1} + (\tau_{ph-e}^{L(T)})^{-1} + (\tau_{DC}^{L(T)})^{-1}, \tag{10}$$

where τ_U, τ_M, τ_b, τ_{ph-e}, and τ_{DC} are the umklapp, impurity, boundary, phonon–electron, and dislocation scattering, respectively. Accordingly, the combined phonon scattering process $(\tau_C^{L(T)})^{-1}$ is as follows:

$$(\tau_C^{L(T)})^{-1} = (\tau_N^{L(T)})^{-1} + (\tau_R^{L(T)})^{-1}. \tag{11}$$

The detailed phonon scattering processes are as follows:

2.1 Umklapp scattering

This mechanism involves phonons colliding and transferring momentum to the crystal lattice, resulting in thermal resistance. It becomes more prominent at elevated temperatures and higher phonon frequencies, which is given by:[35,39]

$$\left[\tau_U^{L(T)}\right]^{-1} = \frac{\hbar(\gamma^{L(T)})^2}{M(v^{L(T)})^2 \theta_D^{L(T)}} \left(\frac{k_B}{\hbar}\right)^2 x^2 T^3 e^{-\left(\frac{\theta_D^{L(T)}}{3T}\right)} \tag{12}$$

where $(\gamma^{L(T)})$ represents the longitudinal (transverse) Gruneisen parameters, and their values are given by $\gamma^L(\infty) = 0.3$ and $\gamma^T(\infty) = 0.22$. These values were determined by fitting theoretical LTC to the experimental data from the bulk state of $In_{0.53}Ga_{0.47}As$.

2.2 Normal scattering

Normal phonon scattering involves phonons being deflected by interactions that preserve their wave vector and net momentum.

This scattering type is often overlooked compared to umklapp processes, and is computed based on:[35,39]

$$(\tau_N^L)^{-1} = \frac{k_B{}^3(\gamma^L)^2 V}{M\hbar^2(v^L)^5}(\omega^L)^2 T^3, \quad (13)$$

$$(\tau_N^T)^{-1} = \frac{k_B{}^4(\gamma^T)^2 V}{M\hbar^3(v^T)^5}\omega^T T^4. \quad (14)$$

2.3 Boundary scattering

The surfaces and interfaces of nanofilms play a crucial role in phonon scattering. Phonons can be reflected or absorbed at these boundaries, according to:

$$\left[\tau_b^{L(T)}\right]^{-1} = \frac{v^{L(T)}}{l}. \quad (15)$$

2.4 Defect scattering

The presence of defects in the lattice can scatter phonons, affecting LTC. The strength of this scattering is contingent upon the material's dispersion curves. The Rayleigh scattering theorem elucidates the interactions between high-frequency phonons and three distinct defect types: impurities (foreign atoms), isotopes, and alloy disorder parameters:[40,41]

$$(\tau_M^{L(T)})^{-1} = \frac{3V^2S^2}{\pi(v^{L(T)})^3}N_{imp}\omega^4 + \frac{V\Gamma}{4\pi(v^{L(T)})^3}\omega^4 + A\times\omega^4. \quad (16)$$

(N_{imp}) represents the concentration of impurities, while (S) denotes the scattering factor, typically around the value of 1. The term for alloy scattering defined at which phonons scatter with the alloy is comparable to the rate of phonon-isotope scattering. The parameter (A) signifies the alloy parameter, which quantifies the intensity of the alloy's scattering effect,[42] and is calculated by $\left(A_{L(T)} = \frac{V\Gamma}{4\pi(v^{L(T)})^3}\right)$, representing the strength of the mass difference interaction, which for $In_{0.53}Ga_{0.47}As$, is calculated as follows:[43]

$$\Gamma_{In_{0.53}Ga_{0.47}As} = 2\left[\frac{(1-X)M_{In}{}^2\Gamma_{In} + XM_{Ga}{}^2\Gamma_{Ga}}{((1-X)M_{In} + XM_{Ga} + M_{As})^2}\right]. \quad (17)$$

2.5 Phonon–electron scattering

In semiconductors and other materials with free electrons, interactions between phonons and electrons can scatter phonons, influencing LTC. Zou and Balandin suggested a method for calculating the rate at which phonons scatter with electrons:[44]

$$\left[\tau_{ph-e}^{L(T)}(x)\right]^{-1} = \frac{N_e E^2 x}{\rho(v^{L(T)})^2\hbar}\sqrt{\frac{\pi m^*(v^{L(T)})^2}{2k_B T}}\exp\left(-\frac{m^*(v^{L(T)})^2}{2k_B T}\right). \quad (18)$$

N_e represents the density of electrons in the conduction band, E denotes the deformation potential with an approximate value of −7.79 eV,[45] m^* symbolizes the effective mass of an electron, which is ($0.041 \times m_e$)[46] for $In_{0.53}Ga_{0.47}As$, where m_e is the resting mass of an electron, and ρ stands for the mass density.

2.6 Dislocation scattering

The rate at which phonons scatter off dislocations, considering a dimensionless parameter for short-range interactions, is determined based on ref. 40 and 41:

$$\left(\tau_{DC}^{L(T)}(x)\right)^{-1} = \eta N_D \frac{V_0^{\frac{4}{3}}}{(v^{L(T)})^2}\left(\frac{k_B T}{\hbar}\right)^3 x^3. \quad (19)$$

In this context, η represents the weight factor, which is assigned a value of 0.55, and N_D denotes the total concentration of dislocations, encompassing both edge and screw types. Factors influencing phonon scattering: several factors can significantly affect phonon scattering processes in nanofilms:[47] in nanofilms, the aforementioned scattering processes can lead to a reduction in LTC compared to bulk materials. This is attributed to the increased surface-to-volume ratio, which amplifies the impact of surface scattering mechanisms. Additionally, confinement effects can alter the phonon spectrum, leading to changes in LTC. An understanding of these processes and their dependencies is crucial for the design of materials with tailored thermal properties.

2.7 Nanofilm dependencies: pressure and size factors

The aforementioned principle can be used when there is no pressure. Considering pressure, which is an important parameter and affects most properties of solids, the model can be applied to the effect of pressure on LTC in $In_{0.53}Ga_{0.47}As$ thick and nanofilms of up to 11 GPa, with modifications of other thermophysical properties, including melting temperature. The bulk solid's melting temperature, $T_m(r,P)$, dependent on pressure, is calculated using the Clapeyron equation:[23,24,48]

$$T_m(r,P) = T_{m0}(r) \times \sqrt{1 + \frac{2(V_l(r) - V_s(r))P + \left(V_s(r)K_s(r) - V_l(r)\left(\frac{\sigma_{sl}(r)}{f_{sl}(r)}\right)K_l(r)\right)P^2}{H_m(r)}}. \quad (20)$$

The Clapeyron equation, in its simplified form (first-order approximation) as a function of size and pressure, allows for easier calculations and can still provide a general understanding of phase behavior, which is useful for nanofilms, calculating the melting temperature.[23,24] T_{m0}, using variables: molar volume V_s and V_l, for solid and liquid states, respectively. Here, V_s is the product of the zero-pressure lattice volume V and Avogadro's number N_A,[23] while V_l is 90% of V_s. Compressibility K_s, and K_l are defined as ($K_s = 1/B$), where B is the bulk modulus, and K_l is typically ten times K_s, and H_m is the melting enthalpy. Surface energy σ_{sl} and stress f_{sl} are critical thermodynamic parameters (Table 1), particularly for calculating $T_m(P)$.

The bulk (thick film in this work) structure surface energy σ_{sl} in eqn (20) is calculated according to the Gibbs–Thomson equation:[24] $\sigma_{sl}(\infty) = \frac{2hS_{vib}(\infty)H_m(\infty)}{3V_s(\infty)R}$, and for nanosized

Table 1 Parameters are obtained through equations stated in the text for both the bulk and nanofilms of $In_{0.53}Ga_{0.47}As$

Material parameters	Thick films 1.4 μm (bulk)	Nanofilm thickness 70 nm	30 nm	20 nm	10 nm
B (GPa)	58.0666	56.8123	55.1463	53.6953	49.383
V_s ($cm^3\ mol^{-1}$)	15.215	15.3861	15.6263	15.8417	16.5187
K_s ($10^{-12}\ Pa^{-1}$)	17.2216	17.6018	18.1335	18.6263	20.2499
B'	1.986	1.99026	1.99606	2.00129	2.01785
v^{ave} ($m\ s^{-1}$)	3237.18	3220.51	3197.6	3176.93	3111.11
γ^{ave}	0.159678	0.1617	0.1646	0.1673	0.1755
K_l ($10^{-12}\ Pa^{-1}$)	172.216	176.018	181.335	186.263	202.499
ρ ($kg\ m^{-3}$)	5541.07	5477.65	5393.45	5320.11	5102.06
V_l ($cm^3\ mol^{-1}$)	13.693	13.8475	14.0637	14.2576	14.8669

films, it is modified to:

$$\sigma_{sl}(r) = \frac{2hS_{vib}(r)H_m(r)}{3V_s(r)R}, \quad (21)$$

where (∞) and (r) denote both bulk state (the thick film) and nanofilms, h is the first solid surface monolayer and calculated from the relation $h = 1.429d_{mean}(\infty)$,[49] and S_{vib} is the material's vibrational entropy obtained from $S_{vib} = S_m - R$.[29] $d_{mean}(\infty)$ is the mean bond length, and it is dependent on the thickness, where $S_m(\infty)$ and R are the melting entropy and the gas constant, respectively. $S_m = H_m/T_m$,[29] where H_m is the melting enthalpy, and for a tetrahedral compound semiconductor it is calculated from this relation:[50] $H_m(\infty) = -10^{-5}T_m^2(\infty) + 0.059T_m(\infty) - 21.33$. Its modification for nanosize-dependent solids can be expressed as:

$$H_m(r) = -10^{-5}T_m^2(r) + 0.059T_m(r) - 21.33. \quad (22)$$

The intrinsic surface stress f_{sl} in eqn (20) is the pressure effect on the surface creating a lattice contraction and it is a reversible work per unit area, which is calculated according to:[30] $f_{sl}(\infty) = \left(\frac{h}{2}\right)\sqrt{\frac{3S_{vib}(\infty)H_m(\infty)}{K_s(\infty) \times V_s(\infty) \times R}}$, for nanofilms, the form is modified to:

$$f_{sl}(r) = \left(\frac{h}{2}\right)\sqrt{\frac{3S_{vib}(r)H_m(r)}{K_s(r) \times V_s(r) \times R}}. \quad (23)$$

The bulk modulus B for the bulk value is calculated from $B(\infty) = v_{ave}^2(\infty)\,\rho(\infty)$, and its nanosize-dependent modification is:[31]

$$B(r) = v_{ave}^2(r)\,\rho(r) \quad (24)$$

Additionally, the average phonon group velocity for the bulk state is $v_{ave}(\infty) = \left[\frac{\left(v^L(\infty)\right)^{-3} + 2\left(v^T(\infty)\right)^{-3}}{3}\right]^{-\frac{1}{3}}$,[51] and its nanosized modification is as in the following:

$$v_{ave}(r) = \left[\frac{\left(v^L(r)\right)^{-3} + 2\left(v^T(r)\right)^{-3}}{3}\right]^{-\frac{1}{3}}, \quad (25)$$

where v^L and v^T are the longitudinal and transverse phonon group velocities, respectively. At the nanoscale, the deflection or reflection of phonons depends strongly on the size. The mean bond length $d_{mean}(\infty)$ at high temperature is an average distance for a phonon. Its change according to the nanosize scale $\Delta d_{mean}(r)$ is given by:[49]

$$\Delta d_{mean}(r) = \Delta d_{mean}(r_c)\left[\exp\left(\frac{-2(S_m(\infty) - R)}{3R\left(\frac{r}{r_c} - 1\right)}\right)\right]^{1/2}, \quad (26)$$

where r is half of the nanofilm thickness, and r_c is the critical radius at which the material melts at zero Kelvin and calculated by $r_c = (3 - D)h$, where D is 0, 1, 2 and 3 for nanoparticles, nanowires, nanofilms and the bulk state (thick films), respectively. For nanofilms, $r_c = h$, $\Delta d_{mean}(r_c)$ in eqn (26), which is the maximum increase in the mean bond length calculated from:[49]

$\Delta d_{mean}(r_c) = h - d_{mean}(\infty)$, and then for nanofilms, the size-dependent mean bond length $d_{mean}(r)$ is calculated according to the relation:

$$d_{mean}(r) = h - \Delta d_{mean}(r). \quad (27)$$

The nanosize-dependent lattice parameter $a(r)$ is calculated from the relation: $a(r) = \frac{4}{\sqrt{3}}d_{mean}(r)$.[49] Accordingly, the lattice volumes for both bulk and nanosize dependence of cubic zinc blende shape structures including $In_{0.53}Ga_{0.47}As$ are calculated from relations $V(\infty) = \frac{a(\infty)^3}{8}$ and $V(r) = \frac{a(r)^3}{8}$, respectively.[52,53] The nanostructure mass density $\rho(r)$ is calculated from the size-dependent lattice volume $V(r)$ of a nanofilm according to $\rho(r) = \rho(\infty)\frac{V(\infty)}{V(r)}$,[31] where $\rho(\infty)$ and $V(\infty)$ are the mass density and lattice volume for the bulk value. The bulk density is given by $\rho(\infty) = \frac{M}{V(\infty)}$, where the average atomic mass M for $In_{0.53}Ga_{0.47}As$ can be calculated as:[43]

$$M = \frac{(1 - X)M_{In} + XM_{Ga} + YM_{As}}{(1 - X) + X + Y}. \quad (28)$$

Hence, $Y = 1$ and $X = 0.47$, and the average atomic masses for In, Ga, and As are abbreviated as M_{In}, M_{Ga}, and M_{As}, respectively. These are calculated from the relation $m_{ave} = \sum_i c_i M_i$, where c_i is the natural abundance of the isotope composition and M_i is the ith isotope atomic mass, with values of 60.107%, 39.89%, 4.33%, 95.67%, and 100% for ^{69}Ga, ^{71}Ga, ^{113}In, ^{115}In, and ^{75}As, respectively.[35] Accordingly, their average atomic mass is equal to 139.95×10^{-27} kg. The size-dependent melting temperature $T_{m0}(r)$ is given by:

$$T_{m0}(r) = T_{m0}(\infty)\left(\frac{V(r)}{V(\infty)}\right)^{2/3}\exp\left(\frac{-2(S_m(\infty) - R)}{3R\left(\frac{r}{r_c} - 1\right)}\right), \quad (29)$$

where for $In_{0.53}Ga_{0.47}As$, $T_{m0}(\infty)$ is 1373.15 K.[54] According to eqn (20), the dependence of both bulk state, the thick film in this case, and nanosize melting temperature on pressure is calculated as shown in Fig. 3 (Fig. 3–11 in Appendix A).

At the nanoscale, the Debye temperature, denoted as θ_D, is key to understanding atomic vibrations in lattice structures.

Table 2 Calculated parameters for $In_{0.53}Ga_{0.47}As$ in both its thick (bulk) and nanofilms

Parameters	Thick films 1.4 μm (bulk)	Nanofilm thickness			
		70 nm	30 nm	20 nm	10 nm
f_{sl} (J m^{-2})	6.30066	6.14814	5.94479	5.76818	5.24622
H_m (kJ mol^{-1})	40.8304	40.6086	40.3077	40.0397	39.2079
σ_{sl} (J m^{-2})	1.67367	1.62881	1.56884	1.5169	1.3644
S_{vib} (J mol^{-1} K^{-1})	21.42	21.1963	20.8895	20.6138	19.7435
S_m (J mol^{-1} K^{-1})	29.734	29.5054	29.1986	28.9229	28.0526

It is calculated using Lindemann's formula: $\theta_D(r) = \theta_D(\infty)\left[\frac{T_m(r)}{T_m(\infty)}\right]^{\frac{1}{2}}$. This formula also applies to the pressure dependence of θ_D for both bulk and nanosize materials:[29]

$$\theta_D(r,P) = \theta_D(r,\infty)\left[\frac{T_m(r,P)}{T_m(r,\infty)}\right]^{\frac{1}{2}}. \quad (30)$$

Fig. 4 shows the nanosize Debye temperature–pressure dependence of $In_{0.53}Ga_{0.47}As$. Phonon group velocity in nanofilms ($v(r)$) is derived from Debye temperature $\theta_D(r)$ proportionality: $v(r) = v(\infty)\frac{\theta_D(r)}{\theta_D(\infty)}$,[28] with $v(\infty)$ being 4260 m s^{-1} for longitudinal and 2981 m s^{-1} for transverse branches.[55] This relationship is modified for pressure dependence (Fig. 5):

$$v(r,P) = v(r,\infty)\frac{\theta_D(r,P)}{\theta_D(r,\infty)} \quad (31)$$

These calculations are also utilized for zero-pressure size-dependent parameters for both thick (bulk state) and nanofilm thicknesses, as detailed in Tables 1 and 2.

Lattice contraction in bulk (thick film) and nanosizes, due to pressure $a^P(r,\infty)$, is described by the Murnaghan equation:[25]

$$a^P(r,\infty) = a(r,\infty)\left[1 + P\left(\frac{B'(r,\infty)}{B(r,\infty)}\right)\right]^{\frac{1}{3B'(r,\infty)}} \quad (32)$$

For $In_{0.53}Ga_{0.47}As$ semiconductor nanofilms and bulk thickness, $a(r,\infty)$ is the zero-pressure lattice parameter, and ($a^P(r,\infty)$) is the pressured lattice parameter, while B' determines the first derivative of the bulk modulus. This investigation uses the Murnaghan equation to find that lattice parameter density, and volume decrease with increasing pressure. Changes in pressure affect the size, shape, and bulk modulus (B) of nanoscale solids, indicating material resistance and hardness.[56,57] The formula for the first derivative of the bulk modulus for cubic materials at ambient pressure is specified:[32] $B' = \frac{5}{3} + 2B\sum v_{ave}\frac{\frac{\partial v_{ave}}{\partial P}}{\sum (v_{ave})^2}$. When pressure derivatives are equal, the first derivative of the bulk modulus is given by the free-volume equation:[32] $B' = \frac{5}{3} + 2\gamma_{th}$, for $\gamma_{th} = \gamma_{ave}$. In this work, the first derivatives of the bulk moduli for bulk thickness and its corresponding nanoscales are derived as follows:

$$B'(r,\infty) = \frac{5}{3} + 2\gamma_{ave}(r,\infty). \quad (33)$$

Then according to eqn (32), the bulk and nanoscale lattice parameter and volume dependence on pressure are as shown in Fig. 6. The average Gruneisen parameter γ_{ave} in eqn (33) is influenced by nanoscale size and pressure, calculated as: $\gamma_{ave} = \left[\frac{(\gamma^L)^{-3} + 2(\gamma^T)^{-3}}{3}\right]^{-\frac{1}{3}}$.[51] Rice[26] derived an equation for the pressure-dependent Gruneisen parameter ($\gamma_P(\infty)$), which is: $\gamma_P(\infty) = \frac{V_P(\infty)}{V(\infty)} \times \left(\left(1 - \frac{V_P(\infty)}{V(\infty)}\right) + \frac{1}{\gamma(\infty)}\right)^{-1}$; this equation accounts for pressure effects on the lattice volume of nanoscale solids.

$$\gamma_P(r) = \frac{V_P(r)}{V(r)} \times \left(\left(1 - \frac{V_P(r)}{V(r)}\right) + \frac{1}{\gamma(r)}\right)^{-1}. \quad (34)$$

The term $V_P(r)$ indicates the effect of pressure on nanoscale lattice volume and is estimated by: $V_P(r,\infty) = V(r,\infty)\left[1 + P\left(\frac{B'(r,\infty)}{B(r,\infty)}\right)\right]^{\frac{1}{B'(r,\infty)}}$. Fig. 7 illustrates how this impacts the Gruneisen parameters for both thick (bulk) and nanofilm materials.

Based on eqn (1)–(34), pressure influences the thermodynamic and structural parameters in the LTC-modified equation for both bulk (thick) and nanofilms, as depicted in Fig. 1.

3. Results and discussion

In LTC calculations for bulk and nanofilms, parameters such as lattice volume, Debye temperature, and group velocity are derived from eqn (20)–(34). Other parameters, like surface roughness and electron concentration, are determined by fitting to the experimental data[5,20] at 0 GPa. Excluding dislocations, the concentration of imperfections, such as impurities (N_{imp}) and electrons (N_e), remains constant across nanosizes and under varying pressures; these values, along with size- and pressure-dependent parameters, eqn (20)–(34), cause modifications in this model, specifically tailored to the properties of $In_{0.53}Ga_{0.47}As$ nanofilms, where ($N_e = 0.8 \times 10^{25}$ m^{-3}) and ($N_{imp} = 0.069 \times 10^{23}$ m^{-3}), and these values are obtained from the fitting process to the experimental data[5,20] of LTC for phonon–electron and phonon-impurity scattering rates, which are inserted into $(\tau_{ph-e}^{L(T)})^{-1}$ and $(\tau_M^{L(T)})^{-1}$ in eqn (10).

New values for the first derivative, appropriate for $In_{0.53}Ga_{0.47}As$ nanofilms, have been determined through a fresh derivation of the nanomaterial form (refer to Table 1). This approach was initially utilized by Hofmeister in 2002 for bulk materials.[32]

Fig. 1 illustrates how hydrostatic pressure affects the LTC of $In_{0.53}Ga_{0.47}As$ nanofilms and bulk (thick film) with a thickness range from 10 nm to 1.4 μm, highlighting phonon-based heat transfer in this semiconductor alloy.

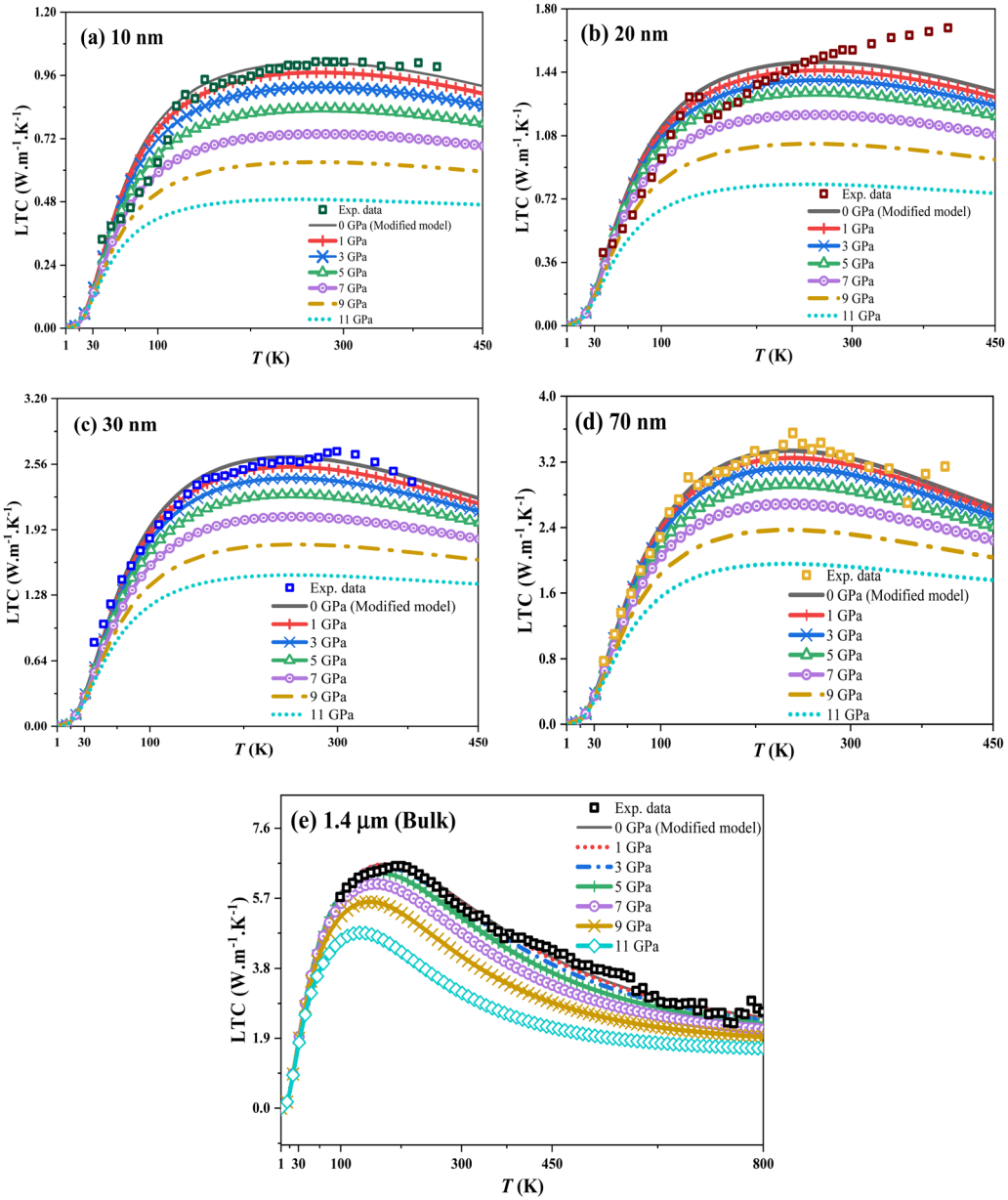

Fig. 1 LTC of $In_{0.53}Ga_{0.47}As$ alloy nanofilms and bulk dependent on temperature under hydrostatic pressure from 0 to 11 GPa for (a) 10 nm, (b) 20 nm, (c) 30 nm, and (d) 70 nm, and (e) 1.4 μm bulk state, respectively, with experimental data for nanofilm thicknesses obtained from ref. 5, and for bulk (thick) from ref. 20.

At low temperatures, phonon wavelengths match the sample size, affecting boundary scattering. As temperature rises, LTC peaks and is influenced by imperfections like dislocations. Electron numbers and impurity concentrations remain unchanged despite size reduction. At higher temperatures, energetic lattice vibrations and short-wavelength phonons (*via* the umklapp process) scatter with the crystal lattices, impacting LTC, as depicted in Fig. 1a–e. Fig. 1a–e show that hydrostatic pressure decreases LTC across all temperatures for $In_{0.53}Ga_{0.47}As$ nanofilms (10–70 nm) and bulk (1.4 μm). At low temperatures (1–30 K), phonons carry minimal thermal energy, making LTC less pressure-dependent. Boundary scattering, influenced by pressure, temperature, and size, is the key factor here. At the nanoscale, phonons are disrupted, and while their excitation energies rise with temperature, pressure diminishes this effect. Pressure effects on LTC are attributed to lattice rearrangement and reduced dislocation lines, especially in 10 nm nanofilms, lowering the LTC peak and increasing scattering, which diminishes the right-side peak of the LTC curve. Increased pressure leads to higher lattice scattering at sample boundaries, reducing phonon group velocities (Fig. 5); the effects are shown in Fig. 8(a) and (b), and both are obtained from the boundary scattering rate in the nanofilm: $[\tau^{L(T)}_{Boundary}]^{-1} = \frac{v^{L(T)}}{l_{eff}}$, where $l_{eff} = \left(\frac{(1-\varepsilon)}{l_c(1+\varepsilon)} + \frac{1}{l}\right)^{-1}$, l_c is the Casimir length, and l is

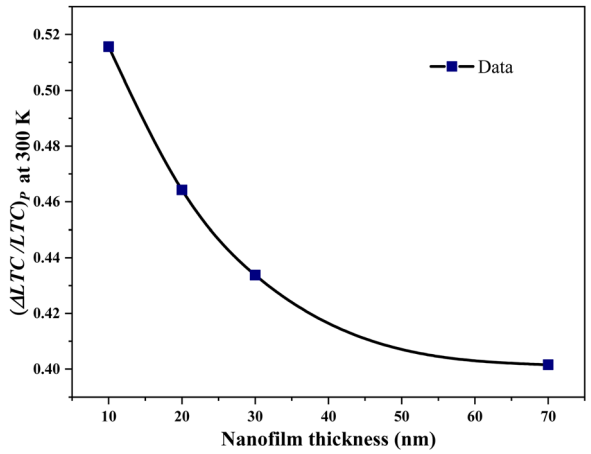

Fig. 2 The dependence of $(\Delta LTC/LTC)_P$ on nanofilm thickness at 300 K.

the sample size,[40] which at 0 GPa equals to 2.61, 2.62, 2.63, 2.64, and 2.8 μm for 10, 20, 30, 70 nm, and 1.4 μm as the bulk, respectively. Surface roughness (ε) ranges from 0 to 1, with $\varepsilon = 0$ for bulk thickness (complete diffusion) and $\varepsilon = 1$ for nanofilms (total reflection). For nanofilms of 10, 20, 30, and 70 nm, the ε values are 0.089, 0.076, 0.069, and 0.054, respectively. Phonon velocities decrease with pressure, more so in thinner films, affecting the $In_{0.53}Ga_{0.47}As$ nanofilms' LTC. Fig. 8(a) and (b) illustrate the inverse relationship between sample thickness and boundary scattering rate. Boundary scattering significantly affects thermal resistivity, more so in strained samples (10 nm). Hydrostatic pressure modifies this rate, reducing LTC, especially at low to intermediate temperatures. It also limits the phonon wavelengths, increasing scattering effects. Despite fewer dislocations, pressure impacts LTC reduction, as shown in Fig. 8(c). From the dislocation scattering rate formula, the N_D (dislocation concentration) values are 4.97×10^{17}, 4.53×10^{17}, 4.27×10^{17}, 3.75×10^{17} and 1.84×10^{17} m^{-2} for 10, 20, 30, 70 nm, and 1.4 μm (thick) bulk, respectively, and they are used to fit LTC to the reported experimental data. The basic assumption is that at intermediate temperatures, boundary scattering has a minor role, while lower dislocation concentration becomes the main factor in thermal energy transfer under pressure. Strained lattices scatter high-energy phonons, affecting LTC as the atom distances decrease under pressure. Smaller sizes see more impact, likely from bond weakening. The effect of pressure on smaller nanosize elucidates the influence of LTC in thinner films (Fig. 1), which is convenient with ref. 58 and 59. LTC reduction with nanosize decrease is evident in $In_{0.53}Ga_{0.47}As$ nanofilms (Fig. 9). Despite pressure-reducing dislocations, LTC_{max} declines due to boundary scattering's greater influence compared to dislocations.

To investigate the pressure's impact on the thermal properties of the $In_{0.53}Ga_{0.47}As$ alloy's nanosize, the LTC at the turning point temperature due to pressure, $T_{tp\ LTC}(P)$, is plotted against pressure in Fig. 10. The LTC at this point is influenced by boundary and lattice dislocation at low and intermediate temperatures. As size compression increases, so does boundary scattering, which outweighs the reduction in lattice dislocations. Increased pressure significantly lowers LTC in thinner films due to a greater reduction in lattice structure and volume, with a pronounced effect in smaller nanofilms, as shown in Fig. 2 and 11.

4. Conclusions

(1) It is expected from this work that the concentrations of both impurities and electrons will remain the same as those in the bulk, unchanged by both effects of nanoscale dimensions and pressure.

(2) Clapeyron, Murnaghan and Post equations were successfully applied within the modified Debye–Callaway model to assess the effects of hydrostatic pressure on the film's lattice thermal conductivity (LTC), considering surface energy and stress.

(3) At a low temperature range, the reduced LTC due to pressure $(\Delta LTC/LTC)_P$ is a strongly temperature-dependent parameter that approaches its minimum value at temperatures above $T = 100$ K. It is also a size-dependent parameter, increasing from its minimum value at low temperatures to a maximum value at room temperature.

(4) The insights gained in this work could be crucial for optimizing the thermal properties of nano thermoelectric devices, potentially improving their functionality and efficiency.

Data availability

The data that support the findings of this study are available from the corresponding author upon reasonable request.

Conflicts of interest

The authors have no conflicts to disclose.

Appendix

Fig. 3–11.

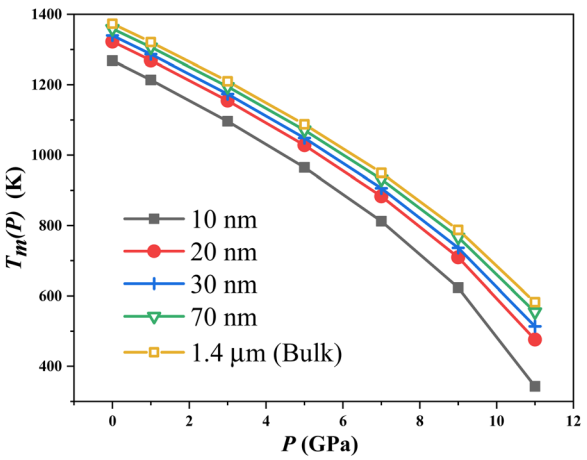

Fig. 3 Melting temperature as a function of pressure for $In_{0.53}Ga_{0.47}As$ films up to 11 GPa.

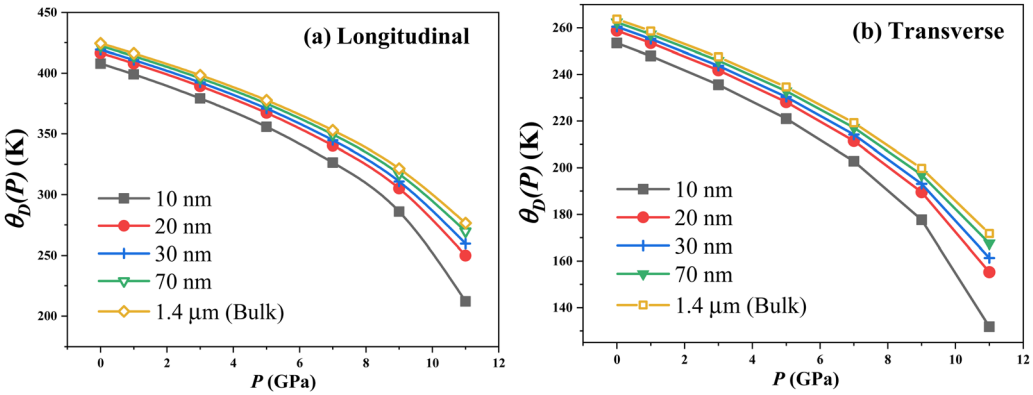

Fig. 4 (a) Longitudinal and (b) transverse modes for Debye temperature as a function of pressure for $In_{0.53}Ga_{0.47}As$ films up to 11 GPa.

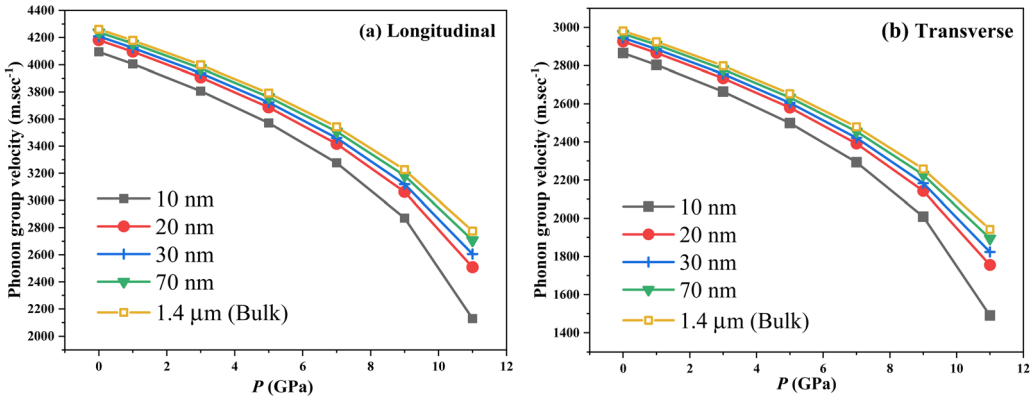

Fig. 5 Phonon group velocity dependent on pressure for $In_{0.53}Ga_{0.47}As$ alloy films for (a) longitudinal and (b) transverse modes, for both thick (bulk) and nanofilms.

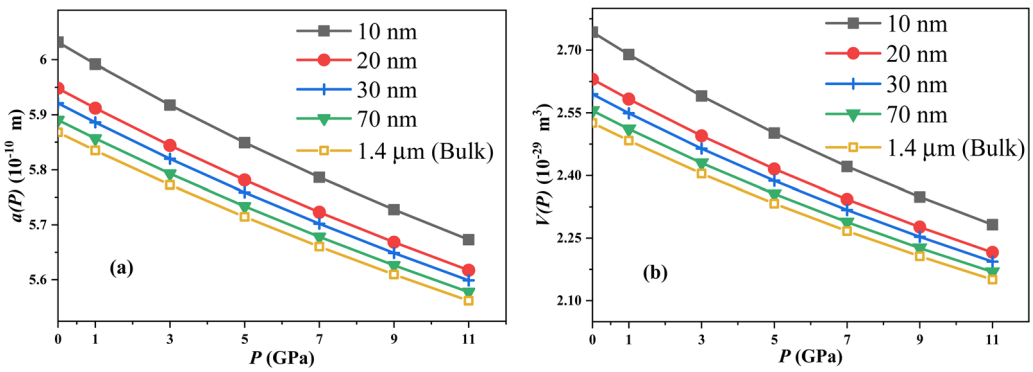

Fig. 6 Pressure-dependent (a) lattice parameter, and (b) lattice volume, for $In_{0.53}Ga_{0.47}As$ alloy films of up to 11 GPa.

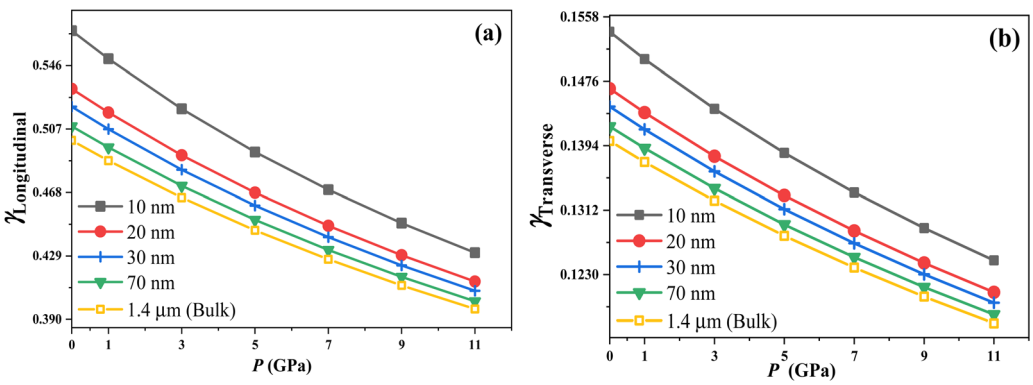

Fig. 7 Gruneisen parameter dependence on pressure for $In_{0.53}Ga_{0.47}As$ alloy films for both modes (a) longitudinal, and (b) transverse.

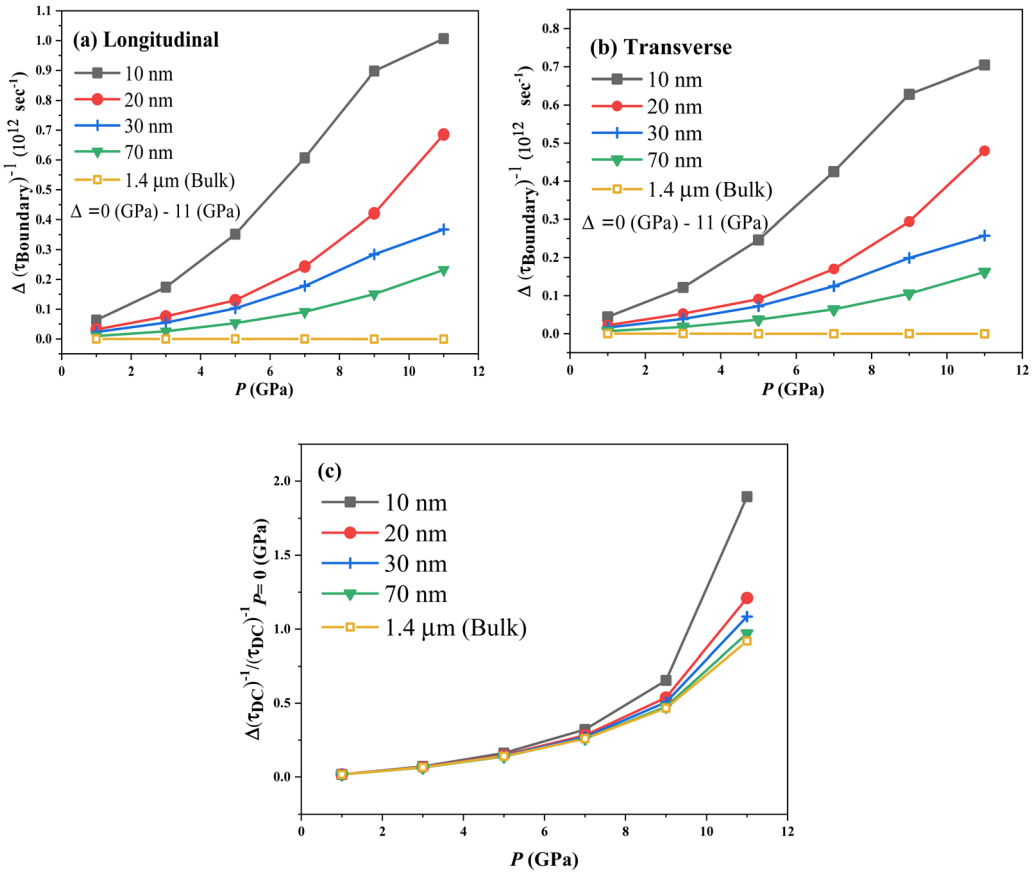

Fig. 8 $\Delta(\tau_{Boundary})^{-1}$ as a function of pressure in (a) and (b), $\Delta(\tau_{Dislocation})^{-1}/(\tau_{Dislocation})^{-1}$ in (c) with different thicknesses of 10, 20, 30, and 70 nm and the bulk state for the $In_{0.53}Ga_{0.47}As$ alloy.

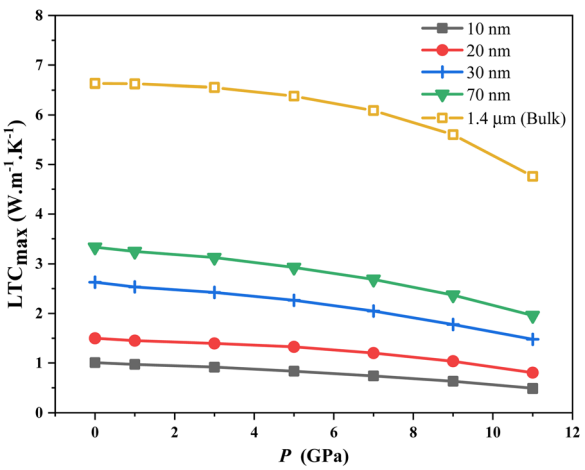

Fig. 9 LTC_{max} as a function of pressure for $In_{0.53}Ga_{0.47}As$ nanofilms with different thicknesses of 10, 20, 30, and 70 nm and bulk (thick).

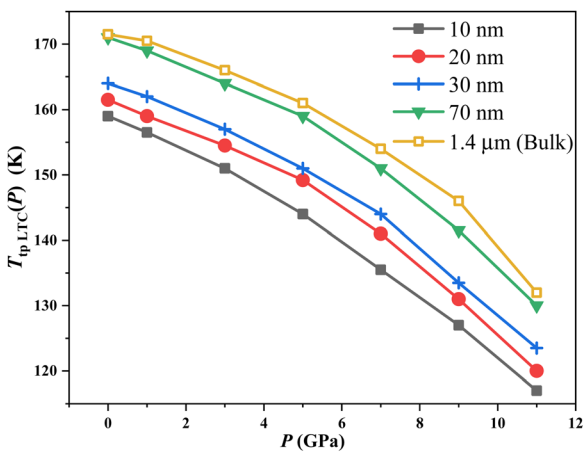

Fig. 10 The turning point temperature for LTC as a function of pressure for $In_{0.53}Ga_{0.47}As$ alloy films.

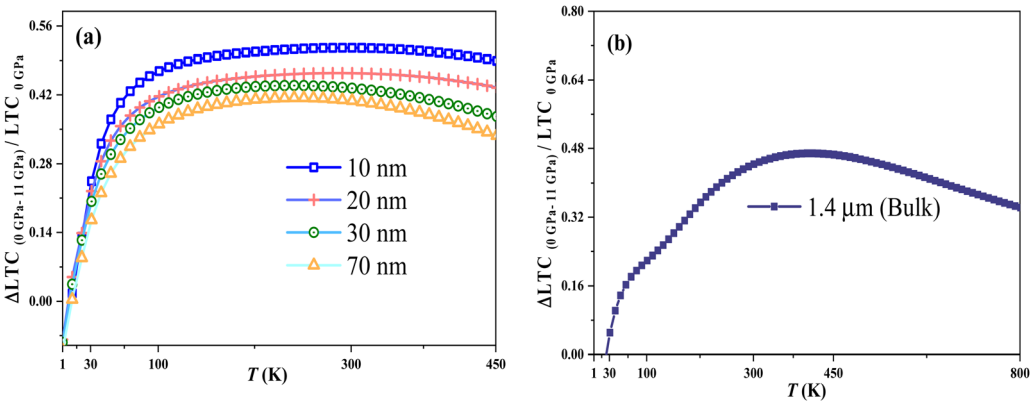

Fig. 11 $(\Delta LTC/LTC)_P$ as a function of temperature for $In_{0.53}Ga_{0.47}As$ alloy with different thicknesses of (a) 10, 20, 30, and 70 nm, and (b) bulk state.

Acknowledgements

Thanks go to I. N. Qader for his assistance, and the authors would like to acknowledge the financial support under grant no. (3/1/6464-992020) from the College of Science at Salahaddin University-Erbil in Kurdistan Region, Iraq.

References

1 M. S. Gudiksen, L. J. Lauhon, J. Wang, D. C. Smith and C. M. Lieber, *Nature*, 2002, **415**, 617–620.
2 Y. Dong, B.-Y. Cao and Z.-Y. Guo, *Phys. E*, 2015, **66**, 1–6.
3 L. Zhu, X. Tang, J. Wang and Y. Hou, *AIP Adv.*, 2019, **9**, 015024.
4 R. Chau, B. Boyanov, B. Doyle, M. Doczy, S. Datta, S. Hareland, B. Jin, J. Kavalieros and M. Metz, *Phys. E*, 2003, **19**, 1–5.
5 J. Kim, H. Kim, M. Emin Kilic, C. Gayner, R. Koltun, H. Park, A. Soon, J. Bowers, C. Palmstrøm and W. Kim, *J. Appl. Phys.*, 2018, **123**, 245103.
6 G. Chen, *Int. J. Therm. Sci.*, 2000, **39**, 471–480.
7 A. San-Miguel, *Chem. Soc. Rev.*, 2006, **35**, 876–889.
8 P. McMillan, *High Press. Res.*, 2003, **23**, 7–22.
9 B. I. Sharma, *J. Appl. Fundam. Sci.*, 2015, **1**, 7.
10 F. Gao, L. Wen, X. Zhang, Y. Guan, J. Li, S. Zhang and G. Li, *Thin Solid Films*, 2015, **589**, 32–37.
11 T. Pearsall, *IEEE J. Quantum Electron.*, 1980, **16**, 709–720.
12 G. Yang and S.-J. Park, *Materials*, 2019, **12**, 2003.
13 D. Bimberg, N. Kirstaedter, N. Ledentsov, Z. I. Alferov, P. Kop'ev and V. Ustinov, *IEEE J. Sel. Top. Quantum Electron.*, 1997, **3**, 196–205.
14 T. Pearsall, M. Piskorski, A. Brochet and J. Chevrier, *IEEE J. Quantum Electron.*, 1981, **17**, 255–259.
15 S. Anthony, *Ars Technica*, 2015, **23**, 201.
16 E. Dong, B. Liu, Q. Dong, X. Shi, X. Ma, R. Liu, X. Zhu, X. Luo, X. Li and Y. Li, *Phys. B*, 2020, **595**, 412344.
17 H. H. Karim, M. Omar and I. N. Qader, *Phys. B*, 2022, **640**, 414045.
18 M. Hamarashid, M. Omar and I. N. Qader, *Silicon*, 2022, 1–10.
19 I. N. Qader, D. M. Mamand, H. H. Rasul, B. J. Abdullah and M. S. Omar, *Iran. J. Sci. Technol., Trans. A: Sci.*, 2022, 1–14.
20 W. Kim, S. L. Singer, A. Majumdar, J. M. Zide, D. Klenov, A. C. Gossard and S. Stemmer, *Nano Lett.*, 2008, **8**, 2097–2099.
21 A. Cherstvy and A. Kornyshev, *J. Phys. Chem. B*, 2005, **109**, 13024–13029.
22 M. Akaogi, in *Encyclopedia of Geochemistry: A Comprehensive Reference Source on the Chemistry of the Earth*, ed. W. M. White, Springer International Publishing, Cham, 2018, pp. 262–263, DOI: 10.1007/978-3-319-39312-4_301.
23 C. Yang and Q. Jiang, *Scr. Mater.*, 2004, **51**, 1081–1085.
24 Q. Jiang and C. Yang, *Curr. Nanosci.*, 2008, **4**, 179–200.
25 F. D. Murnaghan, *Proc. Natl. Acad. Sci. U. S. A.*, 1944, **30**, 244–247.
26 M. Rice, *J. Phys. Chem. Solids*, 1965, **26**, 483–492.
27 M. Omar, B. J. Abdullah, A. S. Karim and S. K. Jalal, *Silicon*, 2023, 1–8.
28 E. J. Post, *Can. J. Phys.*, 1953, **31**, 112–119.
29 L. Liang and B. Li, *Phys. Rev. B: Condens. Matter Mater. Phys.*, 2006, **73**, 153303.
30 C. Yang, J. Li and Q. Jiang, *Chem. Phys. Lett.*, 2003, **372**, 156–159.
31 B. Abdullah, M. Omar and Q. Jiang, *Sādhanā*, 2018, **43**, 1–5.
32 A. M. Hofmeister and H.-k Mao, *Proc. Natl. Acad. Sci. U. S. A.*, 2002, **99**, 559–564.
33 J.-Y. Wu, P. Huang, Q.-H. Luc, H.-L. Ko, Y.-C. Chiang, H.-C. Yu, M.-Y. Chen and E. Y. Chang, *IEEE Trans. Nanotechnol.*, 2023, **22**, 445–448.
34 M. Asen-Palmer, K. Bartkowski, E. Gmelin, M. Cardona, A. Zhernov, A. Inyushkin, A. Taldenkov, V. Ozhogin, K. M. Itoh and E. Haller, *Phys. Rev. B: Condens. Matter Mater. Phys.*, 1997, **56**, 9431.
35 D. Morelli, J. Heremans and G. Slack, *Phys. Rev. B: Condens. Matter Mater. Phys.*, 2002, **66**, 195304.
36 J. Zou, *J. Appl. Phys.*, 2010, **108**, 034324.
37 D. T. Morelli and G. A. Slack, *High thermal conductivity materials*, Springer, 2006, pp. 37–68.
38 J. Callaway, *Phys. Rev.*, 1959, **113**, 1046.
39 G. A. Slack and S. Galginaitis, *Phys. Rev.*, 1964, **133**, A253.

40 S. Mamand, M. Omar and A. Muhammad, *Mater. Res. Bull.*, 2012, **47**, 1264–1272.
41 W. Kim, J. Zide, A. Gossard, D. Klenov, S. Stemmer, A. Shakouri and A. Majumdar, *Phys. Rev. Lett.*, 2006, **96**, 045901.
42 D. Q. Tran, R. Delgado-Carrascon, J. F. Muth, T. Paskova, M. Nawaz, V. Darakchieva and P. P. Paskov, *Appl. Phys. Lett.*, 2020, **117**, 252102.
43 S. Mei and I. Knezevic, *J. Appl. Phys.*, 2015, **118**, 175101.
44 J. Zou and A. Balandin, *J. Appl. Phys.*, 2001, **89**, 2932–2938.
45 R. People, A. Jayaraman, K. Wecht, D. Sivco and A. Cho, *Appl. Phys. Lett.*, 1988, **52**, 2124–2126.
46 Y. A. Goldberg and N. M. Shmidt, *Handbook Series on Semiconductor Parameters: Ternary and quaternary A3B5 semiconductors*, 1999, vol. 2, p. 62.
47 D. Narducci, G. Cerofolini, M. Ferri, F. Suriano, F. Mancarella, L. Belsito, S. Solmi and A. Roncaglia, *J. Mater. Sci.*, 2013, **48**, 2779–2784.
48 C. Yang, G. Li and Q. Jiang, *J. Phys.: Condens. Matter*, 2003, **15**, 4961.
49 M. Omar, *Mater. Res. Bull.*, 2012, **47**, 3518–3522.
50 M. Omar, *Int. J. Thermophys.*, 2016, **37**, 1–11.
51 E. Post, *Can. J. Phys.*, 1953, **31**, 112–119.
52 M. Omar and H. Taha, *Sadhana*, 2010, **35**, 177–193.
53 M. Omar, *Mater. Res. Bull.*, 2007, **42**, 961–966.
54 M. S. Shur, *Handbook Series on Semiconductor Parameters: Ternary and Quaternary III-V Compounds*, World Scientific, 1996, vol. 2.
55 S. Adachi, *Physical properties of III-V semiconductor compounds*, John Wiley & Sons, 1992.
56 M. Sarwan and S. Singh, *J. Alloys Compd.*, 2013, **550**, 150–158.
57 S. Wang and H. Ye, *Phys. Status Solidi B*, 2003, **240**, 45–54.
58 H. Luo and L. Zhu, *J. Appl. Mech.*, 2015, **82**, 111002.
59 L. Zhu and H. Luo, *J. Alloys Compd.*, 2016, **685**, 619–625.